The PDE6 mutation in the rd10 retinal degeneration mouse model causes protein mislocalization and instability and promotes cell death through increased ion influx

Received for publication, June 13, 2018, and in revised form, August 13, 2018 Published, Papers in Press, August 20, 2018, DOI 10.1074/jbc.RA118.004459

Tian Wang[‡], Jürgen Reingruber[§], Michael L. Woodruff[‡¶], Anurima Majumder[‖], Andres Camarena[‡], Nikolai O. Artemyev[‖], Gordon L. Fain[¶], and Jeannie Chen[‡1]**

*From the [‡]Zilkha Neurogenetic Institute and Department of Physiology and Neuroscience, Keck School of Medicine, University of Southern California, Los Angeles, California 90089-2821, the [§]Institut de Biologie, Group of Computational Biology and Applied Mathematics, École Normale Supérieure, 75005 Paris, France, the [¶]Department of Integrative Biology and Physiology, UCLA, Los Angeles, California 90095-1606, the [‖]Department of Molecular Physiology and Biophysics, Carver College of Medicine, University of Iowa, Iowa City, Iowa 52242, and the **Department of Ophthalmology, Jules Stein Eye Institute, David Geffen School of Medicine at UCLA, Los Angeles, California 90095-7000*

Edited by Henrik G. Dohlman

The retinal degeneration model rd10 contains a missense mutation of the catalytic PDE6 β subunit, which hydrolyzes cGMP in response to light. This model produces cell death more slowly than others caused by PDE6 loss of function, making it of particular interest for studying potential therapeutics. We used morphology, biochemistry, and single-cell physiology to examine the mechanism of rd10 degeneration. Our results show that the mutation produces no alteration of *Pde6b* RNA but does dramatically decrease maximal and basal PDE6 activity, apparently caused by a decrease in protein stability and transport. The enzymatic properties of the remaining mutant PDE6 appear to be nearly normal. We demonstrate that an increase in free cGMP, which would result from decreased PDE6 activity and serve to increase opening of the cGMP-gated channels and calcium influx, is an underlying cause of cell death: degeneration of rd10/*Cngb1*$^{-/-}$ double mutants is slower than the parent rd10 line. Paradoxically, degeneration in rd10/*Cngb1*$^{-/-}$ is also slower than in *Cngb1*$^{-/-}$. This rescue is correlated with a lowering of cGMP content in *Cngb1*$^{-/-}$ retinas and suggests that it may be caused by mislocalization of active PDE6. Single-cell recordings from rd10 rods show that the rates of rise and decay of the response are significantly slower; simulations indicate that these changes are primarily the result of the decrease in PDE6 concentration and rod collecting area. Together, these results provide insights into the complex mechanisms that underlie rd10-mediated retinal degeneration and a cautionary note for analysis of therapeutic interventions.

Genetically inherited retinal degeneration is a common cause of blindness and can result from mutations in a large variety of structural and enzymatic proteins of the photoreceptors (1). Many approaches are presently being used to ameliorate or cure these conditions, including introduction of neuroprotective agents, optogenetic techniques, genetic replacement via viral-vector injection, stem-cell therapies, and the development of retinal prostheses (2). The testing of these approaches is often done in mouse models because of the relative ease of manipulation of the genetics of this species, and because much is already known about the anatomy and physiology of the mouse retina, which resembles that of human peripheral retina (3).

One of the most popular models for therapeutic testing is the rd10 line, first isolated as a naturally occurring mutation at The Jackson Laboratory (4). rd10 is an autosomal missense R560C mutation of the *Pde6b* gene, which produces recessively inherited degeneration of the retina (5). This gene encodes the β subunit of the phosphodiesterase 6 (PDE6) protein, which is essential for the proper functioning of the photoreceptor. The β subunit is one of two catalytic subunits of the PDE6 protein, which together with two inhibitory γ subunits form the effector enzyme of rod phototransduction. Stimulation by light triggers a cascade of reactions leading to the hydrolysis of cyclic guanosine monophosphate (cGMP) by the PDE6, and the resulting change in cGMP concentration directly alters the open probability of membrane channels to produce the electrical response of the photoreceptor. Because of the high cooperativity of cGMP binding to the channel (6–8), any small increase in cGMP levels will have a profound effect on the number of open channels and the cations (Na^+, Ca^{2+}) that flow through them. Humans harboring loss of function *Pde6b* mutations develop retinitis pigmentosa, which begins as night blindness and progresses to total blindness as a function of age (9–12). This disease is recapitulated in the rd10 mouse line wherein the rate of degeneration is relatively slow, such that the retina appears nearly normal for the first 2 weeks but then rapidly deteriorates with the number of photoreceptors markedly decreasing (4, 13–15). This relatively slow rate of degeneration facilitates the analysis of genetic rescue (16) or other therapeutic approaches (17, 18). Previous studies have provided an initial description of

This work was supported by National Institutes of Health Grants EY01844 (to G. L. F.), EY10843 (to N. O. A.), and EY027193, EY027387, and EY12155 (to J. C.). The authors declare that they have no conflicts of interest with the contents of this article. The content is solely the responsibility of the authors and does not necessarily represent the official views of the National Institutes of Health.

[†] To the great regret of his family, friends, and colleagues, Michael Woodruff died on July 22, 2017.

[1] To whom correspondence should be addressed: 1501 San Pablo St., ZNI Rm. 227, Los Angeles, CA 90089. Tel.: 323-442-4479; E-mail: jeannie@usc.edu.

the rd10 degeneration (13, 14) and have shown that phototransduction is abnormal. These studies have not, however, provided much information about the cause of the degeneration.

We have sought to gain a better understanding of the rd10 mutation by combining anatomical, biochemical, and physiological approaches. In this study, we show that the rate of cell death can be markedly reduced if the cGMP-gated channels are also deleted, suggesting that rd10 degeneration depends on functioning channels and is precipitated at least in part by an excess influx of ions, including Ca^{2+} into the outer segments. The PDE6 protein appears to have nearly normal activity but is present at a reduced concentration in rd10 rod outer segments. This reduction appears to be at the protein level because the rd10 mutation did not affect the transcript size or abundance when compared with the WT *Pde6b* transcript. Suction-electrode recordings from the few single rods from which we were able to record light-dependent changes in current show responses with slow onset and decay and are consistent with model calculations based on a lower than normal concentration of PDE6 within the rods. We conclude that degeneration in rd10 rods is produced at least in part by a decrease in PDE6 transport to rod outer segments, resulting in a lower than normal concentration of PDE6. This alteration may in turn lead to a higher than normal cGMP concentration in the outer segment and excess Ca^{2+} entry through the cGMP-gated channels. The *rd10* rods do, however, express some PDE6 with nearly normal enzymatic activity, in contrast to rd1 rods that express no PDE6 at all (19, 20). This difference may explain why degeneration is slower in rd10 mice than in rd1 mice.

Results

Channel knockout delays retinal degeneration in the rd10 mouse

PDE6 mutations have been shown to increase intracellular free-calcium (21), and degeneration can be slowed by deleting cGMP-gated channel genes of rods that exhibit little or no measured PDE6 activity, *i.e.* the crossing of the PDE6 mutant into a channel-knockout genetic background delays rod death (22, 23). To see whether elevation of cGMP at least in part underlies eventual rod death caused by the rd10 mutation, we crossed rd10 mice with *Cngb1* knockout mice, whose retinas degenerate much more slowly than the rd10 retina (Fig. 1*A*). In rd10/*Cngb1*$^{-/-}$ double-mutant mice, the rate of retinal degeneration during the first 4 weeks is similar to that of *Cngb1*$^{-/-}$ retinas (Fig. 1*A*). Quantification of the thickness of the outer nuclear layer, which reflects the number of remaining photoreceptor cell nuclei in 4-week-old mice, is shown in Fig. 1*B*. Our observations are consistent with previous reports showing that the rd10 retina degenerates in a graded pattern from central to peripheral retinas (13, 14). Preventing channel expression had a remarkable and long-lasting effect in prolonging photoreceptor cell survival (Fig. 1*C*). These results are consistent with a mechanism of cGMP-mediated toxicity through opening of a large proportion of the channels and a consequent increase in calcium influx.

rd10 PDE6 is mislocalized and expressed at lower levels

We compared the localization of PDE6 in retinal sections from C57, *Cngb1*$^{-/-}$, and rd10/*Cngb1*$^{-/-}$ mice (Fig. 2*A*). In the C57 retina, both PDE6B and PDE6G immunoreactivity were restricted to outer segments in the photoreceptor-cell layer. This localization pattern was also maintained in the *Cngb1*$^{-/-}$ retina, although the outer-segment structure of these mice was less organized and prone to fragmentation (24). In contrast, the fluorescent signal for PDE6B in the rd10 or the rd10/*Cngb1*$^{-/-}$ double-mutant retina was considerably dimmer and diffusely localized throughout the rod compartments. The signal for PDE6G followed that of PDE6B, a result that suggests mislocalization of the PDE6 holoenzyme. The specificity of the PDE6 antibody staining in rods was demonstrated by the lack of staining in the *Pde6g*$^{-/-}$ retinas, which lack PDE6G and express PDE[2] catalytic subunits at greatly reduced amounts (data not shown) (25). These data show that the rd10 mutation reduced protein expression and altered protein trafficking to or retention within the outer segment.

Missense point mutations in *Pde6b* can lead to reduced protein expression by altering RNA splicing, as was observed in the N605S mutation in *atrd3* mice, which, surprisingly, led to exon skipping (26). We investigated whether the rd10 defect occurred at the transcript level by performing RT-PCR on retinal RNA isolated from heterozygous rd10 (rd10/+, Fig. 2*B*, *lanes 1* and *2*), homozygous rd10 (Fig. 2*B*, *lane 3*), and C57 retinas (Fig. 2*B*, *lane 4*). Four pairs of PCR primers were designed to span the entire coding sequence of *Pde6b*. Both the rd10 and WT C57 retinal cDNA yielded the same predicted sized RT-PCR products for all four pairs of primers, indicating that the WT and the rd10 mutant *Pde6b* transcript were of the same size and suggesting no differences in RNA splicing (Fig. 2*B*).

The rd10 C→T missense mutation destroys a HaeII restriction enzyme site (27). This site is contained within the 708-bp PCR product from primer set 3 (Fig. 2*B*). As can be seen in Fig. 2*B*, *lane 3*, the 708-bp PCR product from homozygous rd10 retina is resistant to HaeII digestion, whereas the WT RT-PCR product was cut (Fig. 2*B*, *lane 4, arrow*). We used this restriction site polymorphism to estimate the relative expression level of WT and rd10 *Pde6b* transcripts in heterozygous rd10 mice by HaeII digestion of the RT-PCR product from primer set 3 (Fig. 2*B*, *lanes 1* and *2*). The signal intensity appeared similar between the HaeII-resistant and HaeII-cleaved PCR products obtained within the linear range of amplification (Fig. 2*C*), indicating similar levels of each transcript in retinas from rd10 heterozygous mice. These results show that the rd10 *Pde6b* transcript is the same size and is expressed at similar levels as the WT *Pde6b* transcript. Together, these data suggest that the decrease in rd10 PDE6B expression occurs post-transcriptionally and points to protein instability as a cause of decreased expression.

[2] The abbreviations used are: PDE, phosphodiesterase; BisTris, 2-[bis(2-hydroxyethyl)amino]-2-(hydroxymethyl)propane-1,3-diol; GC, guanylyl cyclase; GCAP, guanylyl cyclase–activating protein; ANOVA, analysis of variance; ERG, electroretinogram.

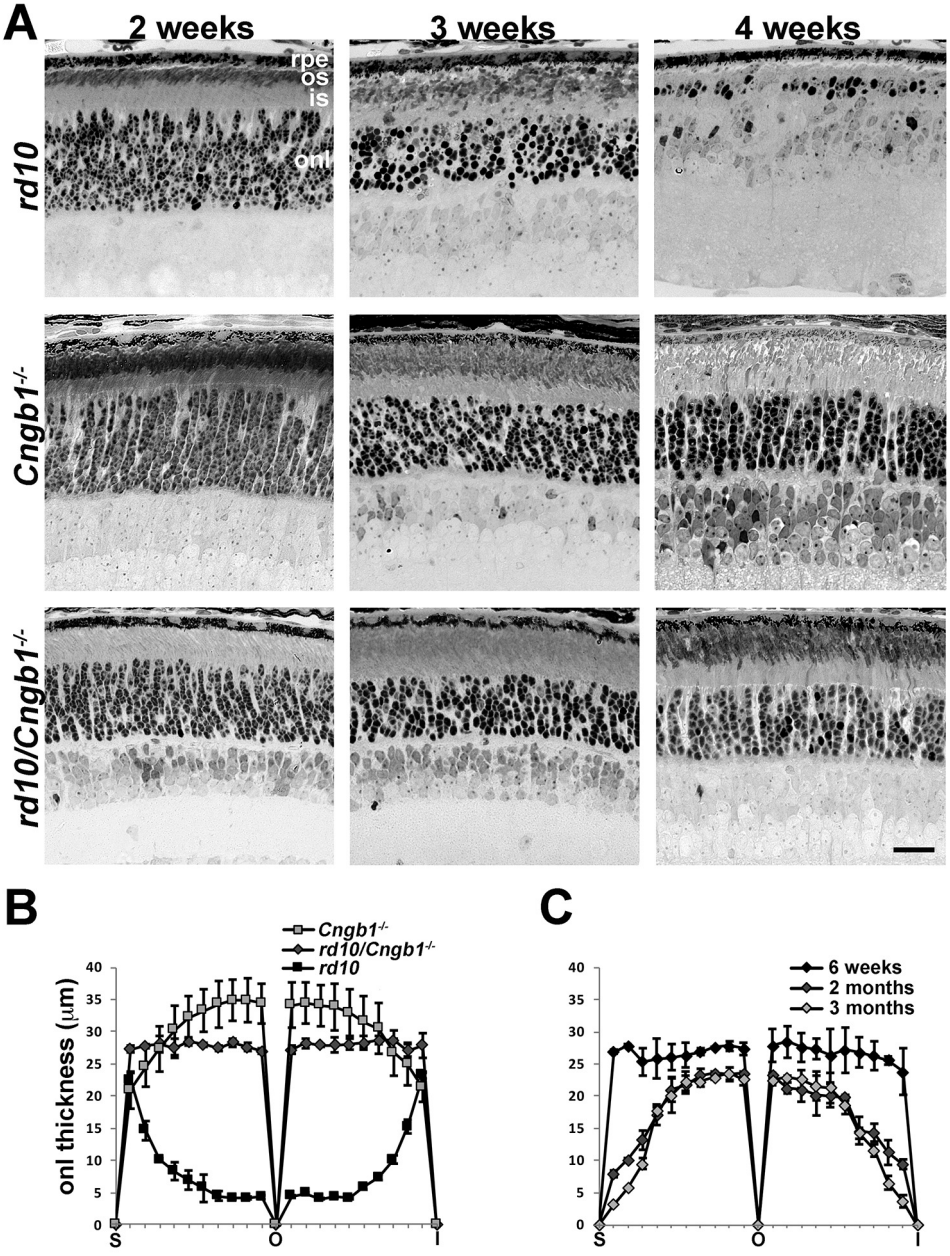

Figure 1. Retinal degeneration in the *rd10* mouse is delayed by preventing expression of the CNG channel. *A,* light micrograph of retinal sections prepared from cyclic light-reared mice of the indicated genotype at 2, 3, and 4 weeks of age. *B,* measurement of outer nuclear layer thickness along the central meridian at 20 locations along the superior (*S*) to inferior (*I*) axis of the indicated mice at 3 weeks of age (mean ± S.D., $N \geq 4$). *C,* outer nuclear layer thickness of *rd10/Cngb1*$^{-/-}$ mice across the span of central retina at 6 weeks (*filled black diamond*), 2 months (*dark gray diamond*), and 3 months (*light gray diamond*) (mean ± S.D., $N \geq 4$). *rpe,* retinal pigmented epithelium; *os,* outer segment; *is,* inner segment; *onl,* outer nuclear layer. *Scale bar,* 20 μm.

We performed Western blots on retinal homogenates to quantify levels of PDE6 (Fig. 3). Retinas collected from 3-week-old mice show that PDE6B in the rd10 and rd10/*Cngb1*$^{-/-}$ samples was reduced when compared with those of C57 and *Cngb1*$^{-/-}$ (Fig. 3*A*). At this age, the retinal thickness was similar between *rd10*/*Cngb1*$^{-/-}$ and *Cngb1*$^{-/-}$ mice (Fig. 1). Therefore, the reduction of PDE6B levels in the *rd10*/*Cngb1*$^{-/-}$ retina relative to that of *Cngb1*$^{-/-}$ suggests that the rd10 mutation affected protein stability.

To obtain more quantitative data, additional Western blots were performed (Fig. 3*B*). Signal intensities of PDE6B and PDE6G were normalized to those of C57 controls (Fig. 3*B*, *bottom*). These normalized values showed a 66% reduction of PDE6B and PDE6G in the *Cngb1*$^{-/-}$ samples and a greater than 90% reduction in rd10 and rd10/*Cngb1*$^{-/-}$ retinas. Interestingly, whereas the ratio of WT PDE6B and PDE6G was close to 1:1 in *Cngb1*$^{-/-}$ retinas, the level of PDE6G appeared to be significantly in excess of PDE6B in the rd10 and rd10/*Cngb1*$^{-/-}$ samples (Fig. 3*B*). Thus, the reduction in PDEB also indirectly led to a decrease in PDE6G expression, albeit not to the same extent.

Strong membrane affinity of PDE6 is conferred by prenylation of the catalytic subunits (28, 29). To see whether mem-

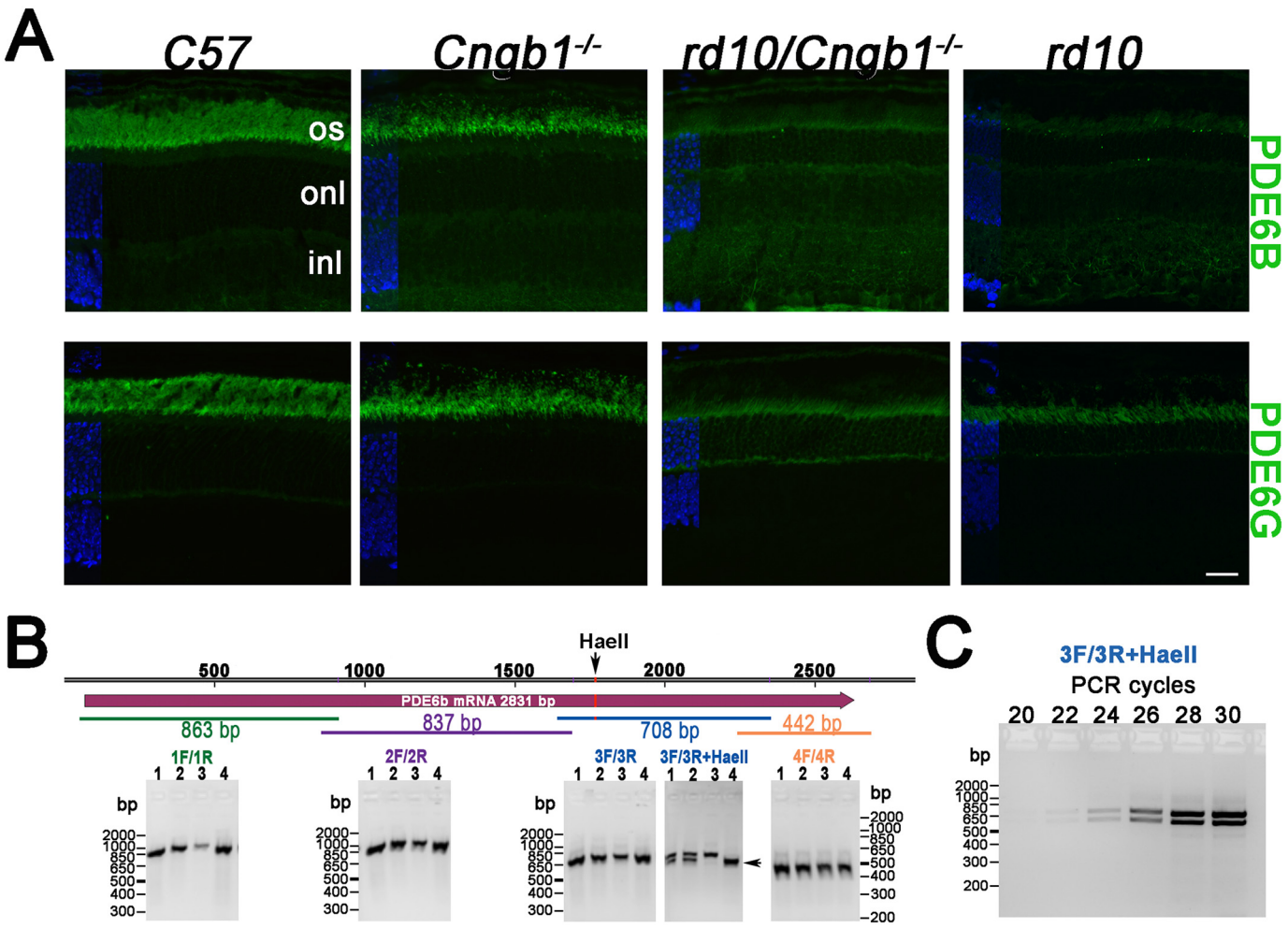

Figure 2. R560C PDE6 mutation affects protein expression and localization. *A,* immunocytochemistry of PDE6B and PDE6G. Expression of both subunits in the C57 and *Cngb1*$^{-/-}$ retina are restricted to the rod outer segment (*os*). In contrast, the rd10 PDE6B mutant along with PDEG are diffusely localized to the inner segment compartments. *os,* outer segment; *onl,* outer nuclear layer; *inl,* inner nuclear layer. *Scale bar,* 20 μm. *B,* rd10 point mutation does not alter transcript size or transcript level. RT-PCR results from total retinal RNA isolated from rd10 heterozygous mice (*lanes 1* and *2*), rd10 homozygous mice (*lane 3*), and C57 mice (*lane 4*). The entire transcript was covered by four overlapping RT-PCR fragments, and their predicted sizes are shown. The rd10 mutation (C⟶T) resides in the 708-bp PCR fragment amplified by primers 3F/3R and destroys the HaeII restriction enzyme site. The *arrow* points to the HaeII-digested fragment from the C57 transcript. *C,* PCR products from primers 3F/3R obtained from different amplification cycles digested with HaeII show similar signal intensity for WT and mutant transcript.

brane association of PDE6 is affected by the rd10 mutation, retinal homogenates were separated into supernatant and pellet fractions and subjected to Western blotting (Fig. 3*C*); the ratio of signal from supernatant to pellet is plotted in Fig. 3*C* (*bottom*). We used rd10/*Cngb1*$^{-/-}$ mice in these experiments because their retinas showed less degeneration and contained a higher level of PDE6. In the C57 and *Cngb1*$^{-/-}$ samples, PDE6B and PDE6G were predominantly in the pellet fraction, as expected for a membrane-associated protein. The ratio of supernatant to pellet was 0.5, which corresponds to 2-fold more protein in the membrane fraction under our experimental conditions (Fig. 3*C*, *bottom*). The mutant rd10 PDE6B was similarly associated with the pellet fraction, suggesting that the mutation did not alter membrane association (Fig. 3*C*, compare *black bars* for C57, *Cngb1*$^{-/-}$, and rd10/*Cngb1*$^{-/-}$). However, the majority of the PDE6G labeling was in the supernatant fraction in the rd10/*Cngb1*$^{-/-}$ samples (Fig. 3*C*, *gray bars*). This result may be partly explained by an excess of PDE6G to PDE6B in the rd10 retina (Fig. 3*B*), but the predominance of PDE6G in the supernatant fraction suggests that the association of PDE6G with rd10 mutant PDE6B may be weaker. This possibility was tested below.

rd10 PDE6 exhibits normal catalytic activity and lowers cGMP in the Cngb1$^{-/-}$ *retina*

To see whether the rd10 mutation affected the interaction of mutant PDE6B with the PDE6G subunit, we assayed inhibition of PDE6 catalytic activity by PDE6G in retinal homogenates from 3-week-old dark-reared rd10 mice (Fig. 4*A*) and compared the values of K_i for retinal samples from each genotype (Fig. 4*B*). The values were not significantly different between experimental groups (one-way ANOVA), suggesting that interaction between PDE6G and PDE6B was not altered. To compare total PDE6 activity present in retinas from different mice, trypsin-activated PDE6 activity (tPDE6) was measured (Fig. 4*C*). Trypsin preferentially cleaves PDE6G from the holoenzyme, thereby providing an estimate of maximal PDE6 activity (30, 31). Trypsin-activated PDE6 activity was slightly reduced

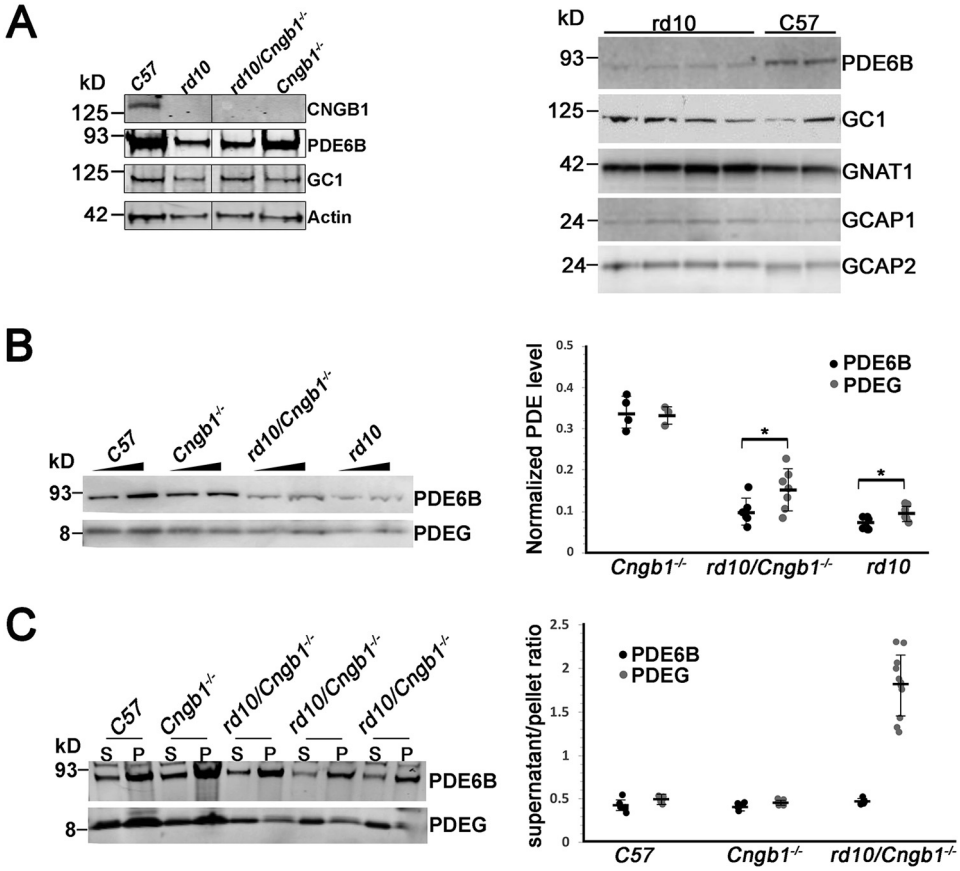

Figure 3. *rd10* PDE6β mutation leads to reduced protein expression and altered PDE6β to PDE6γ subunit ratio. *A,* Western blotting of retinal homogenates from 3-week-old mice show lower PDE6β levels in *rd10* and *rd10/Cngb1*$^{-/-}$ mice, whereas levels of other phototransduction proteins were less affected. The rd10 samples were prepared from dark-reared mice, and similar amounts were loaded per lane (5 μg). *Lanes* from the *left panel* were spliced from the same gel. *B,* representative Western blotting of PDE6β and PDE6γ levels in retinal homogenates prepared from 3-week-old dark-reared rd10 mice. Two protein amounts (5 and 10 μg) were loaded for each genotype. Signals from Western blots were quantified, and values were normalized against that from C57 samples and plotted (mean ± S.D., $N \geq 4$ for all experimental groups). Normalized PDE6β and PDE6γ levels appeared equimolar in the *Cngb1*$^{-/-}$ samples ($p = 0.84$, two-tailed *t* test), whereas a statistical difference (*) was found between *rd10/Cngb1*$^{-/-}$ ($p < 0.05$) and *rd10* samples ($p < 0.02$). *C,* representative Western blots of PDE6β and PDE6γ in fractionated retinal homogenates: *S,* supernatant; *P,* pellet, from the indicated mice. The amounts of protein loaded were as follows: 3 μg (C57), 6 μg (*Cngb1*$^{-/-}$), and 18 μg (rd10/*Cngb1*$^{-/-}$). The ratio of supernatant to pellet signal for both PDE6β and PDE6γ was calculated and plotted at the *bottom* (mean ± S.D., $N \geq 4$ for all experimental groups).

in the *Cngb1*$^{-/-}$ samples (Fig. 4*C*), and in rd10/*Cngb1*$^{-/-}$ samples the PDE6 activity was reduced by ~20-fold. Thus, the rd10 PDE6B mutation reduced the expression of the PDE6 catalytic subunit and shifted the stoichiometry of PDE6B to PDE6G, but it did not affect the interaction of the inhibitory subunit to catalytic subunits. Furthermore, the remaining PDE6 appeared to be functional. This notion is also supported by suction-electrode recording of single rods (see below).

In the dark-adapted retina, cGMP homeostasis is maintained by the opposing action of basal guanylyl cyclase (GC) and basal PDE6 activities. Therefore, we measured basal PDE6 activities in the retinal homogenates from 3-week-old mice (Fig. 4*D*). In rd10 and rd10/*Cngb1*$^{-/-}$ samples, basal activity was reduced by a factor between 10 and 20 (Fig. 4*D*), a somewhat smaller reduction than the maximal PDE6 activity (Fig. 4*C*). To see whether altered basal activity affected cGMP levels, we measured cGMP content in retinas from different dark-adapted mice. In the normal retina, PDE6 sequesters cGMP in its noncatalytic binding sites (GAF domains) thereby acting as a sink for cGMP in the dark-adapted condition (32, 33). For the 3-week-old time point, rd10 retinas from dark-reared mice contained 12 ± 2 pmol/ng protein (mean ± S.D., $n = 3$) *versus* 56 ± 19 pmol/ng (mean ± S.D., $n = 4$) in C57 retinas. Our results suggest that the lower total cGMP in the rd10 retina is due in part to the loss of GAF buffering capacity for cGMP, resulting from degeneration of the photoreceptors, but also in part from the activity of PDE6 remaining in rd10 retinas (Figs. 3 and 4).

Fig. 4*E* shows the levels of cGMP in dark-adapted retinas from 4-week-old C57, *Cngb1*$^{-/-}$, and rd10/*Cngb1*$^{-/-}$ mice. When compared with C57 controls, a significant elevation of cGMP was observed in channel knockouts (Tukey HSD, $p <$ 0.01). This cGMP elevation may result from low outer-segment calcium and continued calcium extrusion via Na^+/K^+–Ca^{2+} exchange (34, 35), leading to stimulation of GC via the guanylyl cyclase–activating proteins (GCAP) (23). Remarkably, the presence of rd10 mutant PDE6 lowered the cGMP level in the rd10/*Cngb1*$^{-/-}$ retinas nearly to that comparable with C57 retinas (Tukey HSD, $p = 0.2$, Fig. 4*E*), despite having less PDE6 activity when compared with WT PDE6 (Fig. 4, *C* and *D*). The lower cGMP content cannot be explained by low PDE6 levels (see "Discussion").

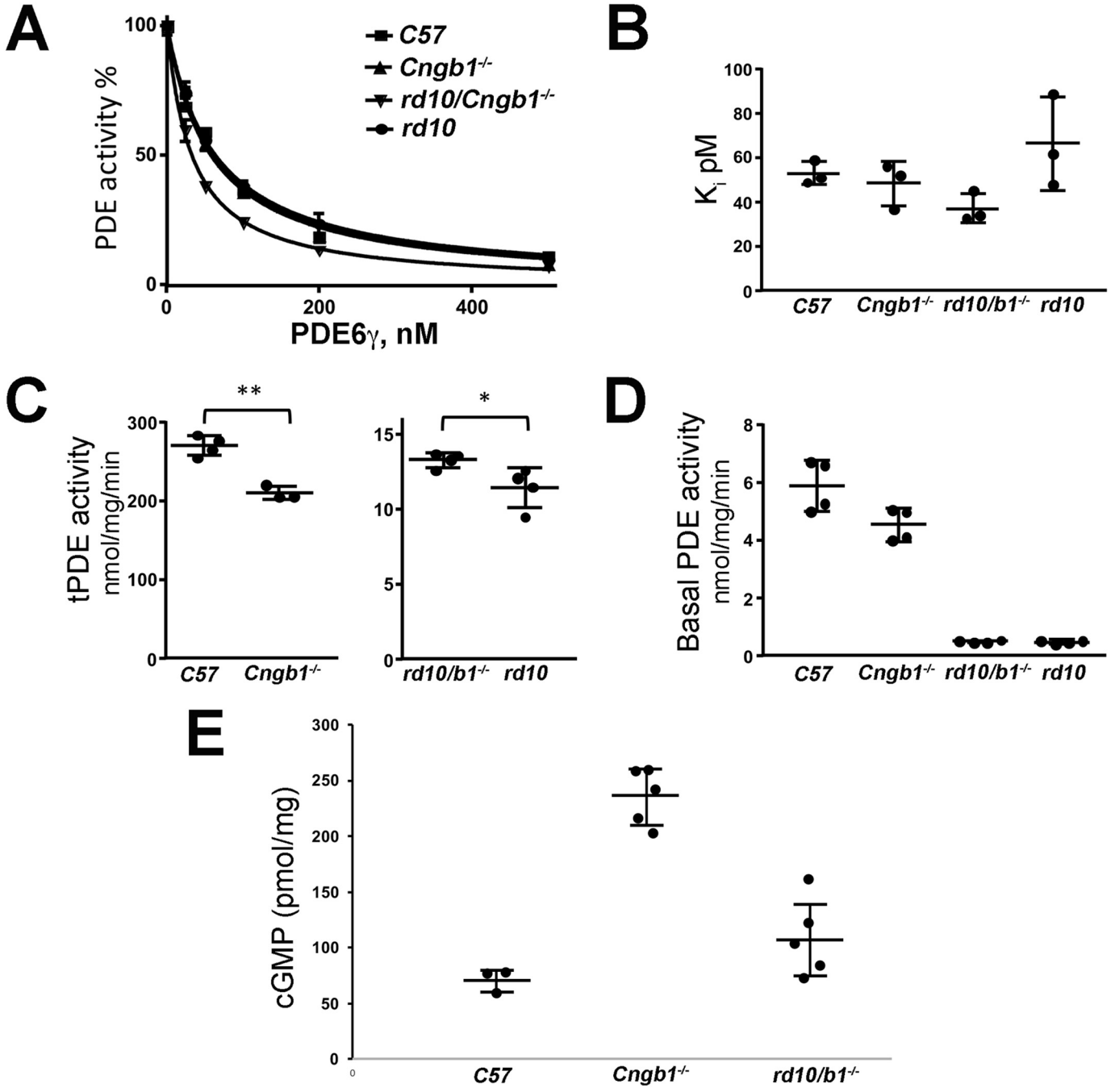

Figure 4. *rd10* PDE mutant shows elevated basal activity and lowers cGMP in *Cngb1*$^{-/-}$ retina. The scatterplots show individual data point from independent experiments and mean and standard deviation values. *A,* titration of PDE activity in retinal homogenates reconstituted with recombinant PDE6γ. *B,* comparison of K_i values for PDE activity in retinal homogenates from the indicated mice. The values were not statistically significantly different by one-way ANOVA. *C,* total PDE activity as shown by trypsin-activated PDE activity. The values from *rd10/Cngb1*$^{-/-}$ and *rd10* are replotted in an expanded scale and shown in the *right panel*. *D,* basal PDE activity in retinal homogenates from the indicated mice. *E,* cGMP levels in dark-adapted retinas from 4-week-old mice of the indicated genotype. A significant difference between the group was first detected by one-way analysis of variance (ANOVA, $F < 0.05$). Tukey HSD test showed a significant difference between *C57* and *Cngb1*$^{-/-}$ and between *Cngb1*$^{-/-}$ and *rd10/Cngb1*$^{-/-}$ (*, $p \leq 0.04$; **, $p \leq 0.001$). No statistically significant difference was found between *C57* and *rd10/Cngb1*$^{-/-}$ ($p = 0.2$).

Mutant rd10 PDE prolonged survival of Cngb1$^{-/-}$ *rods*

The paradoxically lower cGMP levels in rd10/*Cngb1*$^{-/-}$ rods may lead to longer rod survival when compared with *Cngb1*$^{-/-}$ rods because of the effect of elevated cGMP and protein kinase G on cell death (35, 36) To test this hypothesis, we examined retinal morphology in age-matched *Cngb1*$^{-/-}$ and rd10/*Cngb1*$^{-/-}$ mice (Fig. 5). The *Cngb1*$^{-/-}$ retina degenerates over the course of 4 months; outer segments from these rods were shortened and disorganized, and at 5 months most of the rods have disappeared (Fig. 5*A*, *upper panel*). In contrast, retinas from age-matched rd10/*Cngb1*$^{-/-}$ mice had more surviving rods with more structurally intact outer segments (Fig. 5*B*, *lower panel*). This rescue is uniform across the span of the retina (Fig. 5*B*). These

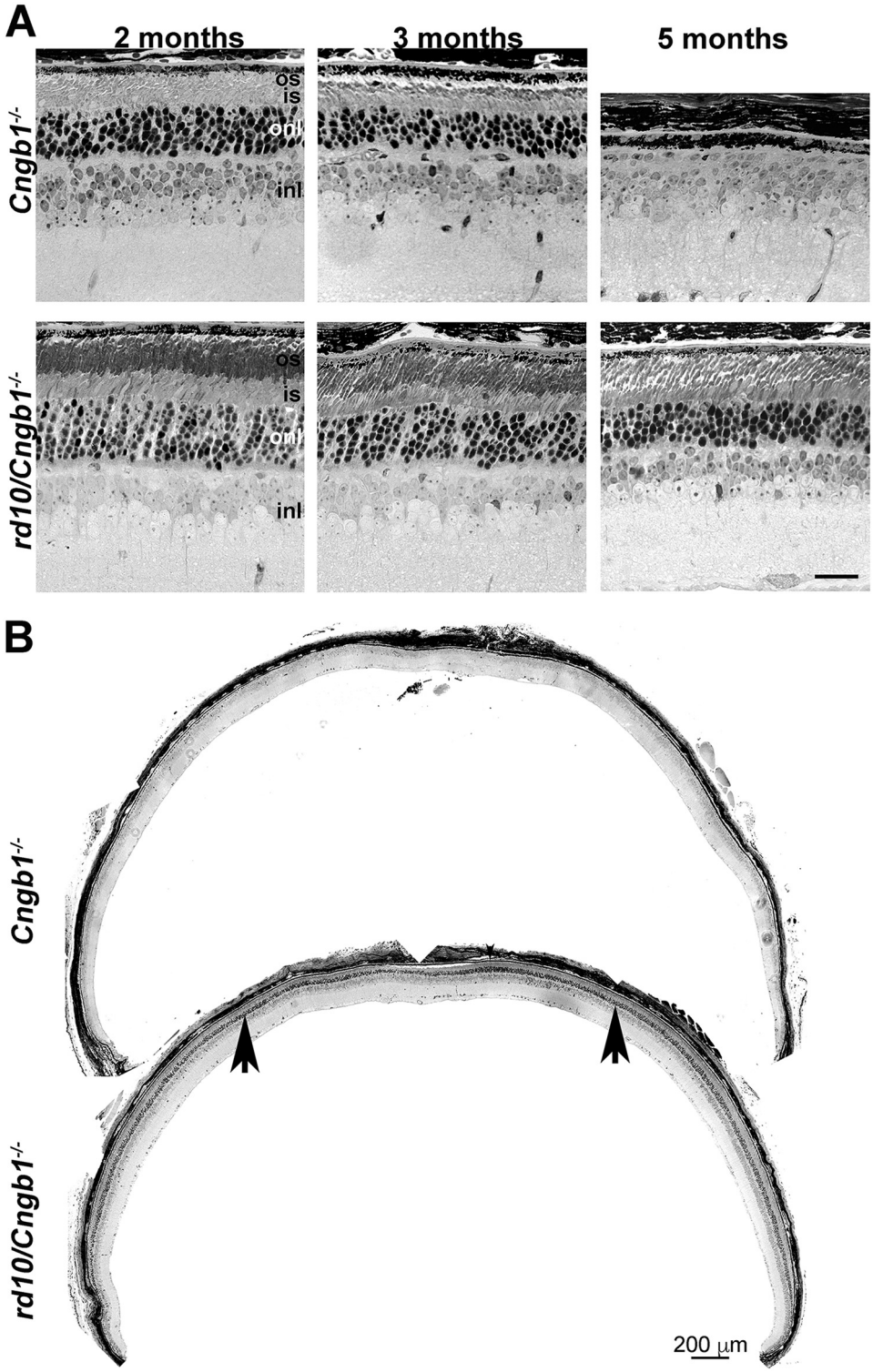

Figure 5. *Pde6b* R560C confers long-term survival to *Cngb1* knockout rods. *A,* time-dependent degeneration in *Cngb1*$^{-/-}$ retinas (*upper panel*) compared with that of age-matched *rd10/Cngb1*$^{-/-}$ retinas (*lower panel*). *Scale bar,* 20 μm. *B,* retinal sections showing the entire span of the retina at the central meridian along the superior (*right*) to inferior (*left*) axis. The *arrows* point to the outer nuclear layer, which is more darkly stained.

results, together with those in Fig. 4*E*, were unexpected, because rd10/*Cngb1*$^{-/-}$ retinas should have less overall PDE6 activity and a higher cGMP concentration than *Cngb1*$^{-/-}$ retinas. We suggest a possible explanation for these findings under the "Discussion."

Responses of rd10 rods

Previous experiments have shown that rd10 animals have at least some functional photoreceptors and show detectable ERGs at least up to 4 weeks of age (13, 15, 18). We therefore attempted to make suction-electrode recordings from single

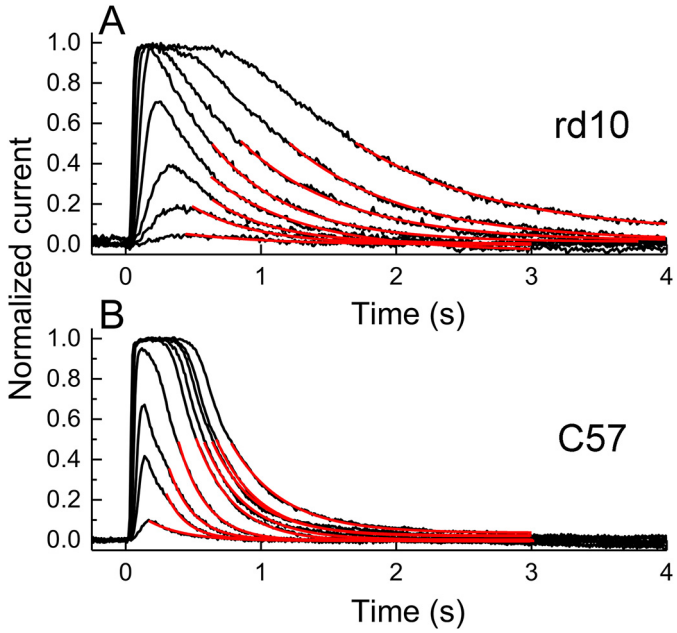

Figure 6. Responses of WT and rd10 rods. *A,* mean responses to 20-ms stimuli from 10 rd10 rods, normalized to mean peak amplitude (for these rods 16.2 pA). Stimuli from dim to bright were as follows (in photons μm^{-2}): 3.9, 17, 43, 159, 453, 645, 863, 1120, and 1870. *Red lines* are single-exponential decay functions that have been fit to the declining phases of the responses. With the exception of the smallest response, fits have been restricted to the region of the response below 0.5 r_{max} to avoid response compression-produced saturation of response amplitude. Time constants from dimmest to brightest were as follows (in ms): 271, 153, 182, 207, 279, 305, 317, 313, and 382. *B,* mean responses to 20-ms stimuli from eight C57 rods, normalized to mean peak amplitude (for these rods 9.85 pA). Stimuli from dim to bright were as follows (in photons μm^{-2}): 2.6, 8.6, 23, 75, 236, 783, 2780, and 9190. *Red lines* are single-exponential decay functions. With the exception of the two smallest responses, fits have been restricted to the region of the response below 0.5 r_{max} to avoid response compression. Time constants from dimmest to brightest were as follows (in ms): 680, 479, 470, 684, 579, 755, 838, and 955.

rods. At 3–4 weeks, mice have small eyes, and they are difficult to dissect. Retinal pieces from rd10 mice had many rods with truncated outer segments often of distorted shape, and many cells had no detectable responses to light. These cells may have been damaged during dissection, but we think it more probable that these were photoreceptors that had already begun to degenerate and had lost light responsiveness. We were nevertheless able to record from a few cells with light responses of nearly normal amplitude. Because we selected cells with the largest responses for our investigation, our sample is unlikely to be representative. These responses may however shed some light on the mechanism of rd10 degeneration.

In Fig. 6*A*, we show mean responses of eight rd10 rods to a series of flashes of increasing intensity, normalized cell-by-cell to the maximum response of each cell (r_{max}). Response waveforms are compared with a normalized flash family of wildtype (WT) C57 rods in Fig. 6*B*, recorded contemporaneously at similar light intensities and published in an earlier study (37). In Table 1, we summarize some of the sensitivity and kinetic parameters of WT and rd10 rods. We could detect no significant difference in maximum response amplitude from the two cell types (r_{max}) or in either of two measures of sensitivity (S_f^D and $I_{½}$), although our sample size was small and variability was larger for rd10 rods than for WT rods. There was, however, a large and highly significant difference in integration time, reflecting the much slower decay of rd10 rods. In Fig. 6, we have fit the declining phases of both rd10 and WT rods to single exponential decay functions at each of the intensities at which measurements were made, restricting the fit to times for which currents were less than half of peak to avoid response compression produced by saturation of response amplitude. The values of the time constants are given in the figure legend. Rods from rd10 retinas decayed on the order of 2–3 times more slowly than WT rods.

This slow decay of the rd10 rod response is probably the result at least in part of decreased expression of outer-segment PDE6, leading to a lower than normal basal activity of PDE6 (Fig. 4*D*) and a lower value of β_{dark}, the dark rate of cGMP turnover (38). It could, however, also result from slower than normal inactivation of light-activated PDE6. To compare rates of decay of light-activated PDE6, we measured τ_D, the limiting time constant (39, 40). The value of τ_D was modestly longer for rd10 rods, and this difference was significant (Table 1). The difference was, however, too small to account for the much slower rate of decline of the rd10 light response.

The rising phases of rd10 responses were also much slower. To quantitate this difference, we have adopted the formulation of Pugh and Lamb (41) and have fit the rising phases of the currents as shown in Equation 1,

$$J(t) = e^{-\frac{1}{2}\Phi t_{fl}\xi A(t - t_{eff})^2} \text{ for } t \geq t_{eff} \qquad \text{(Eq. 1)}$$

where $J(t)$ is the normalized light response; Φ the light intensity in photons $\mu m^{-2}\ s^{-1}$; t_{fl} is the flash duration (20 ms); ξ is the collecting area; A is the amplification constant; and t_{eff} is the effective delay between the beginning of the light flash and the beginning of the photoreceptor response. The collecting area is a proportionality constant that converts the intensity in photons $\mu m^{-2}\ s^{-1}$ into the number of rhodopsins bleached/s and is determined by the volume of the rod, the concentration of rhodopsin, and the quantum efficiency of bleaching, such that $\Phi t_{fl}\xi$ gives the number of rhodopsins bleached by the stimulus. We then define the function $y(t)$ as shown in Equation 2,

$$y(t) = \ln(J(t)) = -1/2\ \Phi t_{fl}\xi A(t - t_{eff})^2 \qquad \text{(Eq. 2)}$$

In Fig. 7, we show $y(t)/\Phi t_{fl}$ as a function of time for WT rods (Fig. 7*A*) and rd10 rods (Fig. 7*B*), with fits obtained from Equation 2, shown as *dashed lines* in Fig. 7*B*. From these fits, we estimated ξA and t_{eff} as 4.6 $\mu m^2\ s^{-2}$ and 24 ms for WT rods. If we assume a value for the collecting area of 0.5 μm^2 (42), A for WT rods would be 9.3 s^{-2}, which is similar to the value previously obtained for WT mouse rods (43). Corresponding values for rd10 rods were $\xi A = 1\ \mu m^2\ s^{-2}$ and $t_{eff} = 21$ ms. The value of ξA was therefore a factor of 4 to 5 lower in rd10 rods. We used these values of ξA to compute the initial time course of the responses, which are shown as *dashed lines* in Fig. 7, *C* and *D*, together with the initial time courses of the responses actually recorded (*continuous lines*).

Simulation of rd10 responses

To obtain a further understanding of the changes occurring in rd10 rods, we have simulated their responses. We began with a model for WT rods (44), similar to previously published mod-

Table 1

Kinetic and sensitivity parameters of WT and Rd10 rods

All values are means ± S.E. Values of maximum response amplitude (r_{max}) were determined cell by cell from responses to saturating flashes; dark-adapted flash sensitivity (S_f^D), by dividing the peak amplitude of the mean dim-flash response for each cell by the flash intensity; the intensity required to produce a half-maximal response ($I_{½}$), from the fit of response-intensity data for each cell to a Boltzmann function in the program Origin; integration time (t_i), from the time integral of the mean dim-flash response for each cell divided by the peak amplitude of the response; response decay constant (τ_{REC}) by fitting a single exponential decay function to averaged responses of small-amplitude (less than 0.3 r_{max}); and the limiting time constant (τ_D) for dark-adapted rods as described under "Experimental procedures." Numbers in parentheses indicate the number of rods recorded.

Animal line	r_{max}	S_f^D	$I_{½}$	t_i	τ_{REC}	τ_D
	pA	*pA photon*$^{-1}$ *μm*^{2}	*photons μm*$^{-2}$	*ms*	*ms*	*ms*
WT (38–47)	14.1 ± 0.6	0.30 ± 0.02	36 ± 3	263 ± 10	214 ± 14	173 ± 10
Rd10 (7–9)	10.7 ± 1.7	0.25 ± 0.07	41 ± 8	656 ± 59	534 ± 104	244 ± 29
t test *p*	0.07	0.53	0.55	0.0001	0.013	0.027

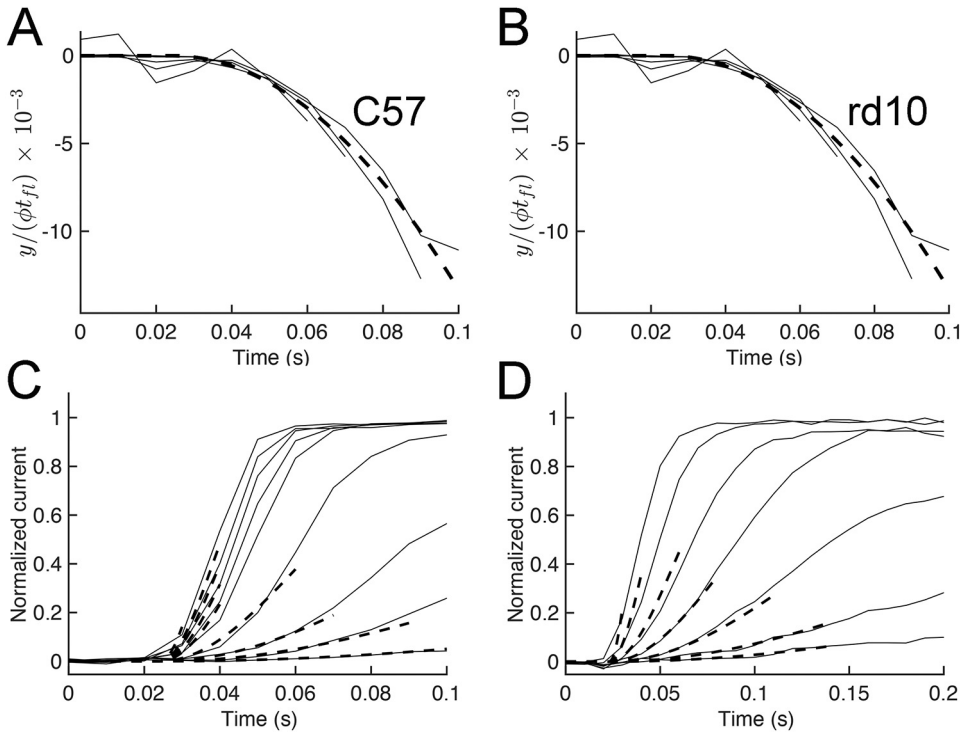

Figure 7. Reduced amplification in rd10 compared with WT rods. *A* and *B* show for WT and rd10 rods the value of $y(t)/\Phi t_{fl}$ (in units of μm^2 photons^{-1}, see Equation 2) computed from WT and rd10 flash families (*solid lines*), together with the best-fitting function $-1/2\ \xi A\ (T - t_{eff})^2$ for $t \geq t_{eff}$ (*dashed lines*). The values of (t_{eff}, ξA) obtained from the fittings were (0.024 s, 4.6 $\mu m^2\ s^{-2}$ photon^{-1}) for WT and (0.023 s, 1.1 $\mu m^2\ s^{-2}$ photon^{-1}) for rd10. *C* and *D*, we compare for WT and rd10 rods the initial waveforms of the mean normalized flash responses from Fig. 5 (*solid lines*) with computed responses (*dashed lines*), obtained by inserting the corresponding values of t_{eff} and ξA into Equation 1.

els for mouse rods (37, 45, 46). We fitted WT normalized responses (Fig. 8*A*) and then used the WT parameters as a starting point to fit recordings of the rd10 flash family. We first determined the impact of modifying only the PDE6 concentration. The simulations showed that reducing PDE6 slows down the rise and decay of the currents in agreement with our recordings; however, the peak amplitudes of the normalized flash responses were systematically larger in the simulations than in the actual responses. A much better fit could be obtained by additionally reducing the rhodopsin concentration, which could be a manifestation of the disorganization of the disks in the rd10 rod outer segments (15).

The simulations in Fig. 8*B* were obtained by reducing the PDE concentration by a factor of about 4 and the concentration of rhodopsin by a factor of about 2. The main effect of the reduced rhodopsin concentration is an effective reduction in the collecting area leading to a reduced rod sensitivity. The reduced PDE concentration had two major effects. First, it decreased the rate of encounter between activated G-protein and PDE6, producing a 4-fold slower rate of decrease of cGMP concentration and channel closure. Second, the reduced concentration of PDE6 produced a lower basal (dark) rate of cGMP hydrolysis (Fig. 4*D*), which in the model simulations of Fig. 8*B* led to an increase in the dark free-cGMP concentration from 4 to 6.4 μM. The increase in cGMP would then cause a larger entry of ions, including Ca^{2+} into the outer segment, increasing the dark Ca^{2+} concentration in our simulations from 0.22 to 0.46 μM. The higher dark cGMP concentration would also have increased the dark current of the rod (r_{max}) by a factor of between 2 and 3, which is in contrast to our experimental observation showing that the recorded value of r_{max} for rd10 rods was not significantly different from the WT value (Table 1). This discrepancy can be accounted for in the model by assuming that the length of the outer segment of an rd10 rod is on average about 2–3 times smaller than WT rods. The rd10 rods from which we made our recordings did indeed have shorter outer

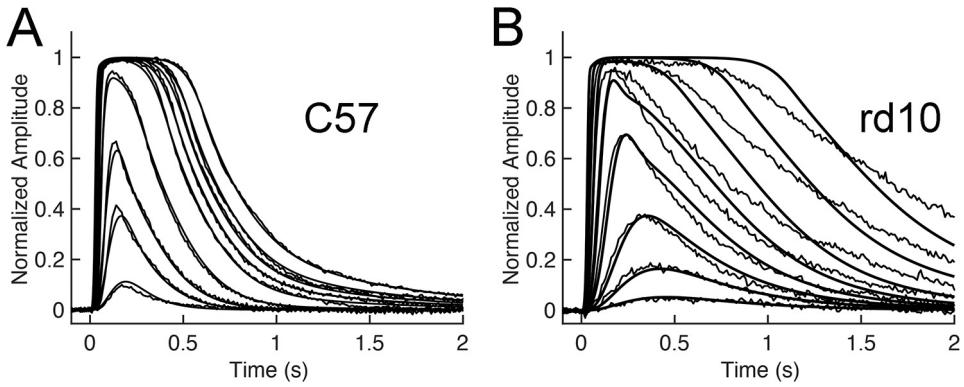

Figure 8. *A,* comparison of recordings (noisier traces) and simulations (*smooth curves*) of flash family responses in a WT rod. *B,* similar comparisons for flash family responses in an rd10 rod. The simulations for *B* were obtained with the same parameters as in *A* except that the PDE concentration was reduced by 4 and the collecting area by 2.

segments but were often bent over and distorted in shape; moreover, only a fraction of the outer segment of the rod may have been functional. Reducing the length of the outer segment decreases the dark current because there is less membrane surface through which ions can flow, but it does not change the time course of the normalized currents shown in Fig. 8*B*. This is because any decrease in rod length would decrease the number of rhodopsins bleached but also increase the rate of hydrolysis of cGMP (β_{sub}), which is inversely proportional to outer segment volume (41).

In summary, the simulations in Fig. 8*B* were produced by assuming WT values for all of the different parameters of response activation and inactivation except for these three: the concentration of PDE6, which was reduced by about 4; the concentration of rhodopsin, which was reduced by about 2; and the length of the outer segment, which was reduced by 2 to 3. No other changes were made. The decrease in PDE6 concentration is likely to be a direct effect of the mutation, probably resulting from the decrease in expression and mislocalization of the enzyme (Fig. 2). but the changes in rhodopsin concentration and length of the outer segment seem more likely to result from the ensuing degeneration. The fits at dim intensities leading up to saturation were remarkably close to the recorded responses. At brighter intensities and longer times, the simulations increasingly diverged from the recordings, probably as the result of other changes occurring in the rd10 rods. Because of our uncertainty about the nature of these changes, we made no further attempt to improve the fits.

Discussion

The rd10 mutation was first described as a retinal degeneration resulting from a missense mutation of the PDE6 β subunit, which produces cell death more slowly than rd1 or some other mouse models of retinitis pigmentosa (4). We have used morphology, biochemistry, and single-cell physiology to investigate the mechanism of the rd10 degeneration.

Retinal structure, PDE6 expression, and degeneration

Our experiments confirm previous observations (4, 13–15) that retinal structure and photoreceptor number are initially almost normal in the rd10 retina, but that, beginning at about 2–3 weeks of age, degeneration proceeds rapidly in cyclic light-reared mice (Fig. 1, *A–C*). We show further that degeneration can be markedly slowed if the rd10 mutation is combined with *Cngb1*$^{-/-}$ (Fig. 1*A*), which eliminates not only the β subunit of the cyclic nucleotide-gated channel but also the α channel subunit (47, 48) and most if not all outer-segment ion permeability (49). We interpret this result to show that degeneration in rd10 rods is produced at least in part by ion influx, probably by increased entry of Ca^{2+} as for other PDE6 mutations (21–23).

The rd10 retina expresses PDE6 localized to the photoreceptors, although there is substantially less protein than in WT rods, and the remaining PDE6 is largely mislocalized to the inner segment (Fig. 2*A*). The cause of this decrease in protein expression is post-transcriptional (Fig. 2*B*). The good correlation between protein expression level as quantified by Western blots (Fig. 3*B*) and trypsin-activated enzyme activity (Fig. 4*C*) indicates that most, if not all, of the expressed protein is functional. Thus, the R560C mutation likely leads to protein instability and mislocalization. Previous studies have identified the GAFa domain of PDE6 to contain a rod outer segment localization signal (50); the Arg-560 residue is, however, situated at the catalytic domain, which is on opposite end of the molecule and therefore may represent a distinct trafficking signal.

The level of cGMP is substantially elevated in *Cngb1*$^{-/-}$ retinas, a condition likely caused by a persistent low intracellular calcium and constitutive guanylyl cyclase stimulation by calcium-free GCAPs. Elevated cGMP stimulates protein kinase G, contributing to rod death (23). Surprisingly, the R560C PDE6B mutation offered long-term rescue to the *Cngb1*$^{-/-}$ rods (Fig. 5). The rescue lasted beyond 5 months, a time at which all of the *Cngb1*$^{-/-}$ rods have disappeared. This rescue is correlated to a decrease in cGMP content in the rd10/*Cngb1*$^{-/-}$ retinas by comparison to *Cngb1*$^{-/-}$ retinas (Fig. 4*E*). The low cGMP content cannot be explained by low PDE6 expression and loss of noncatalytic cGMP-binding sites, because retinas from *Pde6γ/Cngb1* double-knockout mice, in which PDE6 enzyme is even less abundant and less active, contained similarly high cGMP levels as in *Cngb1*$^{-/-}$ retinas (23). The reason for the ability of rd10 PDE6 to lower cGMP in the *Cngb1*$^{-/-}$ retinas is not entirely clear, but it may be related to the mislocalization of active mutant PDE6 in inner segment compartments where cGMP in *Cngb1*$^{-/-}$ retinas is known to accumulate (51). We

suggest therefore that the rescuing effect of the R560C mutant PDE6 may be related to this mislocalization of active enzyme. If this hypothesis is true, then it would also suggest that, in the *Cngb1*$^{-/-}$ rods, the accumulated cGMP is very compartmentalized and is not accessible to the WT PDE6 in the outer segment of these rods.

The enzymatic properties of the mutant PDE6 appear to be similar in at least some respects to those of WT PDE6 (Fig. 4). The K_i value of PDE6γ inhibition of PDE6 catalytic activity is not significantly different between rd10/*Cngb1*$^{-/-}$ and *Cngb1*$^{-/-}$ retinas (Fig. 4, *A* and *B*), suggesting a normal association between PDE6γ and the catalytic subunits. Moreover, simulations of rd10 light responses at least at dim intensities require only a change in the amount of PDE6 without any change in the enzymatic properties of the enzyme. There are, however, other indications that rd10 mutant PDE6 is not entirely normal. The limiting time constant was longer for rd10 rods than for WT rods, and this difference was significant. Because under the conditions of our experiments the limiting time constant reflects the rate of light-activated PDE6 decay (39, 40), this observation indicates that interactions among PDE6γ, transducin-α–GTP, and the GTPase-activating proteins may be subtly altered.

Responses of rods in rd10 mice

Previous experiments with extracellular ERG recordings have shown that rd10 rods show at least some sensitivity to light (13, 15, 18). We have extended these observations by making single-cell, suction-electrode recordings from dark-reared rd10 retinas. We were able to find some rods in rd10 retinas that responded to light, but responses were highly variable, and many cells did not respond at all. We believe these differences reflect at least in part a variable rate of cell death. This pattern may in turn be the result of variable transport of PDE6 to rd10 rod outer segments.

The responses we recorded showed a much slower rise of the response and a slowed decay (Fig. 6). Our quantitative measurements of the rising phase indicate that the quantity ξA (the collecting area times the amplification constant) is about 4–5 times smaller in rd10 rods than in WT rods (Fig. 7). A decrease in the rate of rise of the rd10 rod response was previously observed in ERG recordings (13) and attributed to a change in the gain of transduction. Our measurements indicate that expression of PDE6 is reduced, which would slow the rate of rise of activation in proportion to the decrease in PDE6 concentration; however, our simulations indicate that there is likely also to be a decrease in the collecting area ξ attributable at least in part to a decrease in the volume of the rod. Any decrease in rod volume, for example by shortening of the rod outer segment, would increase the rate of decrease of the concentration of cGMP and increase the amplification constant, at least partially compensating the decrease in PDE6 concentration. It is therefore possible that A is nearly unaffected in the rd10 rods and that the decrease in the rate of rise in Fig. 6 may be mostly the result of a decrease in the collecting area.

The rod response also declined much more slowly (Fig. 6), which we attribute in part to a decrease in the rate of turnover of cGMP (β_{dark}) and in part to a slowing of the decay of light-activated PDE6 (τ_D, see Table 1). The changes in the kinetics of rod responses in the rd10 mouse are remarkably similar to those previously reported for hypomorphs of the AIPL1, a protein thought to function as a chaperone for PDE6 (52, 53). Mutant AIPL1 rods with only about 20% of the normal concentration of PDE6 had responses that also rose and decayed more slowly than WT, with a decrease in ξA to about a third of its WT value (53). Responses also decayed more slowly, probably again in part by a decrease in β_{dark} and in part by slowing of the decay of light-activated PDE6 (τ_D was also significantly slower in the mutant AIPL1 rods).

Despite these similarities to rd10, there is one interesting and important difference: the retinas of rd10 mice exposed to cyclic light degenerate much more rapidly than those of AIPL1 hypomorphs, whose photoreceptor layer is nearly intact in animals as old as 3 months (52). One possible explanation of this difference is the much greater variability in PDE6 concentration and rate of degeneration in rd10. It seems possible that many rd10 rods under normal lighting conditions receive little functional PDE6, particularly in the central retina, and that these rods begin to die quite rapidly. Other rods may have some complement of PDE6 and continue to respond to light. The early death of many of the rods may deprive the retina of essential factors, which may precipitate the eventual death of the remainder (54, 55). Total cGMP levels in retinas from 3-week-old dark-reared rd10 mice were lower than in age-matched C57 mice, in contrast to rd1 (56), and Pde6γ knockout mice (25) where cGMP was significantly elevated. This low steady-state cGMP may also help explain why rd10 photoreceptors degenerate more slowly.

rd10 retina as a model system for degeneration

Our experiments indicate that rd10 mice should be used with caution in studies of retinal rescue and repair. Because degeneration is quite variable, conclusions drawn from a partial sampling of retinal morphology or physiology may be difficult to interpret. Our recordings indicate that in the rods whose responses we were able to record, the PDE6 concentration was reduced by no more than a factor of 4, whereas in the retina as a whole the reduction in PDE6 was at least 10-fold (Fig. 3*B*). Our recordings substantiate a decreased concentration of PDE6, but the quantitative decrease in our sample of responding rods is unlikely to be representative of the population of rods taken as a whole. Single-cell and whole-retina measurements of rod physiology are likely to reflect only those rods that can respond, complicating the interpretation of rescue experiments.

The mechanism of degeneration in the rd10 mutation is also likely to be complex and multifactorial. Our experiments show that at least one cause of cell death is a decrease in PDE6 transport into rod outer segments, leading to a decrease in PDE6 activity and an increase in free cGMP and probably Ca^{2+} under a cyclic light–rearing condition. Our experiments show that the degeneration accelerated by illumination is slowed by removing the cGMP-gated channels, implicating a contribution by light-induced increase of cGMP. Interestingly, dark-rearing rd10 mice have been shown to slow degeneration (27, 57, 58). Our observation that cGMP did not accumulate in dark-adapted rd10 retinas may explain this rescuing effect. We hope our

experiments have contributed to a clarification of the mechanism of degeneration in rd10 rods, but we are clearly very far from a complete understanding of this intriguing mutation.

Experimental procedures

Animals

All experimental procedures were performed in accordance with regulations established by the National Institutes of Health and approved by the Institutional Animal Care and Use Committees of the University of Southern California and UCLA. The rd10 mice were obtained from The Jackson Laboratory (Bar Harbor, ME). For some experiments, rd10 mice were bred into the knockout background of *Cngb1* to generate double-mutant mice.

Retinal morphology and measurement of retinal thickness

Mice were anesthetized by isoflurane inhalation and killed by cervical dislocation. Orientation of the eye was marked by cauterization. Enucleated whole eyes were fixed for 5 min in one-half Karnovsky buffer (2.5% glutaraldehyde, 2% formaldehyde in 0.1 M cacodylate buffer, pH 7.2), after which the corneas were cut out with iris scissors and lens removed. The remaining eyecups were further fixed overnight in one-half Karnovsky buffer at 4 °C. The next day, the tissues were rinsed three times for 15 min each in 0.1 M cacodylate buffer and prepared into epoxy resin blocks as described previously (59). The eyecup was hemisected along the superior–inferior axis, and 1-μm–thick central retina sections were collected and stained with Richardson stain for light microscopy. Images were acquired on an Axioplan2 microscope (Zeiss). The thickness of the outer nuclear layer (ONL) was measured as in a previously described method (23). Briefly, each hemisphere was divided into 10 equal segments from the optic nerve to either the superior or inferior tip. At each segment, three independent measurements were made and averaged. Measurements excluded the first 100 μm from the optic nerve due to the thinness of the ONL at this location.

cGMP ELISA

Mice were dark-adapted overnight. Their retinas were isolated under IR light and placed individually into microcentrifuge tubes. The tubes were wrapped in light-tight aluminum foil, immediately frozen in liquid N_2, and stored at −80 °C. On the day of the assay, each frozen retina was homogenized in 100 μl of cold 6% TCA followed by 6 times extraction with 1 ml of water-saturated ether. The aqueous solution was dried in a vacuum centrifuge (UVS 400 Universal Vacuum system). Total cGMP amount was measured with a cGMP XP assay kit (Cell Signaling catalog no. 4360S) according to the manufacturer's instructions.

Western blots

Each isolated retina was homogenized in 150 μl of lysis buffer (150 mM NaCl, 50 mM Tris, pH 8.0, 0.1% Nonidet P-40, 0.5% deoxycholate acid) containing 0.1 mM phenylmethanesulfonyl fluoride and complete miniprotease inhibitor (catalog no. 11836153001, Roche Applied Science). DNase I (30 units, Roche Applied Science) was added and incubated at room temperature for 30 min. The total protein amount of each sample was determined by the BCA™ protein assay kit (ThermoFisher Scientific catalog no. 23227). An equal amount of protein from each sample was electrophoresed on 4–12% BisTris SDS-polyacrylamide gel (Invitrogen), then transferred to nitrocellulose membrane (Whatman catalog no. 10402480), and incubated overnight at 4 °C with the following primary antibodies: rabbit anti-PDE6β polyclonal antibody (1:1000, Cytosignal PAB-06800); rabbit anti-PDEγ polyclonal antibody (1:1000, gift from Dr. V. Arshavsky); mouse anti-GC1 antibody, 1S4 (1:5000, gift from Dr. W. Baehr); mouse anti-CNGB1 antibody 4B1 and anti-CNGA1 antibody PMc1D1 (1:500, gifts from Dr. R. Molday); and mouse anti-actin antibody (1:5000, Millipore MAB1501). The membranes were then incubated with fluorescently labeled secondary antibodies (1:10,000 Li-Cor P/N926-31081) at room temperature for 1 h and detected with an Odyssey IR-imaging system. For the supernatant–pellet fractionation experiment, retinas were homogenized in 200 μl of isotonic buffer (80 mM Tris, pH 8, 4 mM $MgCl_2$, protease inhibitors) and centrifuged for 5 min at 20,000 × *g*. Supernatant was transferred to a new tube, and the pellet was homogenized again in lysis buffer (150 mM NaCl, 50 mM Tris, pH 8.0, 0.1% Nonidet P-40, 0.5% deoxycholate acid, protease inhibitors) followed by DNase I incubation. Different volumes were loaded to enhance visualization of the PDE6 signal (in μl): C57, 2.5 and 5.0; *Cngb1*$^{-/-}$, 5, 10; rd10/*Cngb1*$^{-/-}$, 15, 30; and rd10, 15, 30.

Immunocytochemistry

The anterior segment of the eye was removed as described above, and the remaining eyecup was placed in cold 4% formaldehyde in phosphate-buffered saline (PBS) for 20 min. Fixed tissue was rinsed three times (10 min each) in cold PBS. The eyecups were then cryoprotected in 30% sucrose overnight at 4 °C, embedded in O.C.T.™ (Tissue-Tech®), frozen in liquid N_2, and stored at −20 °C. Frozen sections of 10 μm thickness were prepared with a cryostat (CM 3050 S, Leica Microsystems) and stored at −80 °C. The thawed sections were air-dried and blocked with 2% BSA, 2% goat serum, and 0.3% Triton X-100 in PBS for 1 h. The sections were incubated with either rabbit anti-PDE6β polyclonal antibody (Cytosignal PAB-06800) or rabbit anti-PDEγ polyclonal antibody (gift from Dr. V. Arshavsky) overnight at 4 °C, rinsed, and incubated for 1 h with a fluorescein-labeled or Texas Red–labeled secondary antibody (1:400, Vector Laboratories). The sections were further rinsed and mounted in Vectashield containing 4′,6-diamidino-2-phenylindole (Vector Laboratories). Rhodamine-conjugated peanut agglutinin (Vector Laboratories) was diluted 1:100 in buffer (PBS containing 1 mM $CaCl_2$, 1 mM $MgCl_2$, 1 mg/ml BSA) and incubated on the slides for 1 h at room temperature.

Assays of PDE6 activity and inhibition by PDE6γ

Because dark-rearing slows retinal degeneration in rd10 (27, 57, 58), all samples used in PDE activity assays were from 3-week-old dark-reared rd10 mice to maximize PDE6 levels. Other genotypes were reared under normal cyclic light (12 h light/12 h dark). For each genotype, two mouse retinas were

homogenized by sonication (two 5-s pulses) in 100 μl of 20 mM Tris-HCl, pH 7.5, buffer containing 120 mM NaCl, 1 mM $MgSO_4$, and 1 mM mercaptoethanol. After a brief centrifugation (20,000 $\times$ *g*, 2 min, 4 °C) to remove cell debris, retinal homogenates (typically, 9–10 mg protein/ml) were used to measure basal PDE6 activities with final dilutions of 1:160 for C57 and *Cngb1*$^{-/-}$ retinas and 1:40 for rd10 and rd10/*Cngb1*$^{-/-}$ retinas. Maximal (trypsin-activated) PDE6 activities were measured from retinal homogenates treated with trypsin (100 μg/ml) for 10 min at 25 °C. Trypsin treatment was terminated with the addition of 10$\times$ soybean trypsin inhibitor and incubation for 5 min at 25 °C, followed by centrifugation at 20,000 $\times$ *g* for 3 min at 4 °C. The final dilutions of trypsin-treated retinal homogenates in the assays of maximal PDE6 activity were 1:8000 for C57 and *Cngb1*$^{-/-}$ retinas and 1:400 for rd10 and rd10/*Cngb1*$^{-/-}$ retinas.

To determine the K_i values of PDE6γ inhibition, PDE6 activities in the trypsin-treated samples were also measured in the presence of indicated concentrations of PDE6γ (0–500 pM). PDE6 assays were carried out in 40 μl of 20 mM Tris-HCl, pH 7.5 buffer, containing 120 mM NaCl, 2 mM $MgSO_4$, 1 mM 2-mercaptoethanol, 0.1 unit of bacterial alkaline phosphatase, and 10 mM [^{3}H]cGMP (100,000 cpm) for 10–15 min at 25 °C. The reaction was stopped by the addition of AG1-X2 cation–exchange resin (0.5 ml of 20% bed volume suspension). Samples were incubated for 6 min at 25 °C with occasional mixing and spun at 10,000 $\times$ *g* for 3 min. Then 0.25 ml of the supernatant was removed for counting in a scintillation counter. Groups of measurements were compared with a two-tailed unpaired Student's *t* test.

Analysis of Pde6b transcript by RT-PCR

Total RNA was extracted from one retina of 4-week-old dark-reared C57 (+/+), rd10/+, and rd10/rd10 mice. The RNA was reverse-transcribed and PCR-amplified by using the following primers that cover the entire span of the coding sequence of Pde6b (NM_008806.2). The position of each primer on the *Pde6b* transcript is indicated in parentheses: 1F (49–66) and 1R (893–911); 2F (859–878) and 2R (1678–1695); 3F (1641–1659) and 3R (2329–2348); and 4F (2241–2260) and 4R (2664–2682).

Electrical recording and light stimulation

All recordings from rd10 retinas were from dark-reared mice 3–4 weeks old. Eyes were enucleated under dim red light. The anterior portion of the eye was cut, and the lens and cornea were removed in darkness by means of IR image converters. The retina was isolated from the eyecup and chopped into small pieces with a razor blade. The pieces were then transferred to the recording chamber in complete darkness by means of IR goggles (American Technologies Network Corp.). During recording the photoreceptors were continuously perfused with the same solution used for the dissection, which was Dulbecco's modified Eagle's medium (D-2902, Sigma) supplemented with 15 mM $NaHCO_3$, 2 mM sodium succinate, 0.5 mM sodium glutamate, 2 mM sodium gluconate, and 5 mM NaCl, bubbled with 5% CO_2 in O_2, pH 7.4. Temperature was maintained at 35–38 °C. The recording electrodes were filled with Locke's solution, which contained (in mM) 93 NaCl, 2.1 KCl, 2.6 $CaCl_2$, 1.8 $MgCl_2$, 2.0 $NaHCO_3$, and 10.8 Hepes, pH 7.4. Fire-polished borosilicate glass was pulled with a micropipette puller (P-97, Sutter Instrument), and the tip size was further adjusted under a compound microscope by moving the pipette close to a platinum heating wire.

Responses of single photoreceptor outer segments were recorded with the suction-electrode technique (60). The change in outer-segment membrane current produced by a stimulus was registered with a current-to-voltage converter (Axopatch 200A; Axon Instruments, Inc.), low-pass filtered at 30 Hz with an 8-pole Bessel filter (Kemo Limited Electronic Filters), and sampled at 100 Hz. Cells were stimulated with a dual-beam optical bench; the light of halogen lamp bulbs was passed through electronic shutters (Uniblitz) and interference filters at 500 nm, near the peak of spectral sensitivities of mouse rods (61). The intensity of the light was attenuated with absorptive neutral-density filters, and the light intensity was calibrated with a photodiode (UDT Instruments, San Diego, CA, formerly Graseby Optronics). The values of τ_D in Table 1 were measured as in Chen *et al.* (62) by giving a series of five flashes each between 4 and 7 intensities chosen for each rod to fall within 1.5 log units above the flash intensity that just produced saturation of that rod's response amplitude. The time in saturation (t_{sat}) was measured as the time from the beginning of the flash to the time at which the mean circulating current recovered to 25% of its dark-adapted value. Unless otherwise stated, errors are given as standard errors of the mean (S.E.), and significance was tested with Student's *t* test. Curve fitting, statistical tests, and plotting of data were done with the program Origin (OriginLab Inc., Northampton, MA).

Author contributions—T. W., J. R., M. L. W., A. M., A. C., N. O. A., G. L. F., and J. C. data curation; T. W., M. L. W., A. M., N. O. A., and G. L. F. formal analysis; T. W. and J. R. methodology; J. R. investigation; N. O. A., G. L. F., and J. C. funding acquisition; N. O. A., G. L. F., and J. C. writing-review and editing; G. L. F. and J. C. writing-original draft; J. C. conceptualization; J. C. project administration.

References

1. Rattner, A., Sun, H., and Nathans, J. (1999) Molecular genetics of human retinal disease. *Annu. Rev. Genet.* **33,** 89–131 CrossRef Medline
2. Scholl, H. P., Strauss, R. W., Singh, M. S., Dalkara, D., Roska, B., Picaud, S., and Sahel, J. A. (2016) Emerging therapies for inherited retinal degeneration. *Sci. Transl. Med.* **8,** 368rv6 CrossRef Medline
3. Naarendorp, F., Esdaille, T. M., Banden, S. M., Andrews-Labenski, J., Gross, O. P., and Pugh, E. N., Jr. (2010) Dark light, rod saturation, and the absolute and incremental sensitivity of mouse cone vision. *J. Neurosci.* **30,** 12495–12507 CrossRef Medline
4. Chang, B., Hawes, N. L., Hurd, R. E., Davisson, M. T., Nusinowitz, S., and Heckenlively, J. R. (2002) Retinal degeneration mutants in the mouse. *Vision Res.* **42,** 517–525 CrossRef Medline
5. Wert, K. J., Lin, J. H., and Tsang, S. H. (2014) General pathophysiology in retinal degeneration. *Dev. Ophthalmol.* **53,** 33–43 CrossRef Medline
6. Haynes, L. W., Kay, A. R., and Yau, K. W. (1986) Single cyclic GMP-activated channel activity in excised patches of rod outer segment membrane. *Nature* **321,** 66–70 CrossRef Medline
7. Warren, R., and Molday, R. S. (2002) Regulation of the rod photoreceptor cyclic nucleotide-gated channel. *Adv. Exp. Med. Biol.* **514,** 205–223 CrossRef Medline

8. Zimmerman, A. L., and Baylor, D. A. (1986) Cyclic GMP-sensitive conductance of retinal rods consists of aqueous pores. *Nature* **321,** 70–72 CrossRef Medline
9. Danciger, M., Blaney, J., Gao, Y. Q., Zhao, D. Y., Heckenlively, J. R., Jacobson, S. G., and Farber, D. B. (1995) Mutations in the PDE6B gene in autosomal recessive retinitis pigmentosa. *Genomics* **30,** 1–7 CrossRef Medline
10. Dryja, T. P., Rucinski, D. E., Chen, S. H., and Berson, E. L. (1999) Frequency of mutations in the gene encoding the α subunit of rod cGMP-phosphodiesterase in autosomal recessive retinitis pigmentosa. *Invest. Ophthalmol. Vis. Sci.* **40,** 1859–1865 Medline
11. Hahn, L. B., Berson, E. L., and Dryja, T. P. (1994) Evaluation of the gene encoding the γ subunit of rod phosphodiesterase in retinitis pigmentosa. *Invest. Ophthalmol. Vis. Sci.* **35,** 1077–1082 Medline
12. Huang, S. H., Pittler, S. J., Huang, X., Oliveira, L., Berson, E. L., and Dryja, T. P. (1995) Autosomal recessive retinitis pigmentosa caused by mutations in the α subunit of rod cGMP phosphodiesterase. *Nat. Genet.* **11,** 468–471 CrossRef Medline
13. Gargini, C., Terzibasi, E., Mazzoni, F., and Strettoi, E. (2007) Retinal organization in the retinal degeneration 10 (rd10) mutant mouse: a morphological and ERG study. *J. Comp. Neurol.* **500,** 222–238 CrossRef Medline
14. Barhoum, R., Martínez-Navarrete, G., Corrochano, S., Germain, F., Fernandez-Sanchez, L., de la Rosa, E. J., de la Villa, P., and Cuenca, N. (2008) Functional and structural modifications during retinal degeneration in the rd10 mouse. *Neuroscience* **155,** 698–713 CrossRef Medline
15. Hasegawa, T., Ikeda, H. O., Nakano, N., Muraoka, Y., Tsuruyama, T., Okamoto-Furuta, K., Kohda, H., and Yoshimura, N. (2016) Changes in morphology and visual function over time in mouse models of retinal degeneration: an SD-OCT, histology, and electroretinography study. *Jpn. J. Ophthalmol.* **60,** 111–125 CrossRef Medline
16. Deng, W. T., Sakurai, K., Kolandaivelu, S., Kolesnikov, A. V., Dinculescu, A., Li, J., Zhu, P., Liu, X., Pang, J., Chiodo, V. A., Boye, S. L., Chang, B., Ramamurthy, V., Kefalov, V. J., and Hauswirth, W. W. (2013) Cone phosphodiesterase-6α' restores rod function and confers distinct physiological properties in the rod phosphodiesterase-6β-deficient rd10 mouse. *J. Neurosci.* **33,** 11745–11753 CrossRef Medline
17. Rex, T. S., Allocca, M., Domenici, L., Surace, E. M., Maguire, A. M., Lyubarsky, A., Cellerino, A., Bennett, J., and Auricchio, A. (2004) Systemic but not intraocular Epo gene transfer protects the retina from light-and genetic-induced degeneration. *Mol. Ther.* **10,** 855–861 CrossRef Medline
18. Strettoi, E., Gargini, C., Novelli, E., Sala, G., Piano, I., Gasco, P., and Ghidoni, R. (2010) Inhibition of ceramide biosynthesis preserves photoreceptor structure and function in a mouse model of retinitis pigmentosa. *Proc. Natl. Acad. Sci. U.S.A.* **107,** 18706–18711 CrossRef Medline
19. Bowes, C., Li, T., Danciger, M., Baxter, L. C., Applebury, M. L., and Farber, D. B. (1990) Retinal degeneration in the rd mouse is caused by a defect in the β subunit of rod cGMP-phosphodiesterase [see comments]. *Nature* **347,** 677–680 CrossRef Medline
20. Pittler, S. J., and Baehr, W. (1991) Identification of a nonsense mutation in the rod photoreceptor cGMP phosphodiesterase β-subunit gene of the rd mouse. *Proc. Natl. Acad. Sci. U.S.A.* **88,** 8322–8326 CrossRef Medline
21. Davis, R. J., Tosi, J., Janisch, K. M., Kasanuki, J. M., Wang, N. K., Kong, J., Tsui, I., Cilluffo, M., Woodruff, M. L., Fain, G. L., Lin, C. S., and Tsang, S. H. (2008) Functional rescue of degenerating photoreceptors in mice homozygous for a hypomorphic cGMP phosphodiesterase 6 b allele (Pde6bH620Q). *Invest. Ophthalmol. Vis. Sci.* **49,** 5067–5076 CrossRef Medline
22. Paquet-Durand, F., Beck, S., Michalakis, S., Goldmann, T., Huber, G., Mühlfriedel, R., Trifunović, D., Fischer, M. D., Fahl, E., Duetsch, G., Becirovic, E., Wolfrum, U., van Veen, T., Biel, M., Tanimoto, N., and Seeliger, M. W. (2011) A key role for cyclic nucleotide gated (CNG) channels in cGMP-related retinitis pigmentosa. *Hum. Mol. Genet.* **20,** 941–947 CrossRef Medline
23. Wang, T., Tsang, S. H., and Chen, J. (2017) Two pathways of rod photoreceptor cell death induced by elevated cGMP. *Hum. Mol. Genet.* **26,** 2299–2306 CrossRef Medline
24. Gilliam, J. C., Chang, J. T., Sandoval, I. M., Zhang, Y., Li, T., Pittler, S. J., Chiu, W., and Wensel, T. G. (2012) Three-dimensional architecture of the rod sensory cilium and its disruption in retinal neurodegeneration. *Cell* **151,** 1029–1041 CrossRef Medline
25. Tsang, S. H., Burns, M. E., Calvert, P. D., Gouras, P., Baylor, D. A., Goff, S. P., and Arshavsky, V. Y. (1998) Role for the target enzyme in deactivation of photoreceptor G protein *in vivo*. *Science* **282,** 117–121 CrossRef Medline
26. Muradov, H., Boyd, K. K., Kerov, V., and Artemyev, N. O. (2012) Atypical retinal degeneration 3 in mice is caused by defective PDE6B pre-mRNA splicing. *Vision Res.* **57,** 1–8 CrossRef Medline
27. Chang, B., Hawes, N. L., Pardue, M. T., German, A. M., Hurd, R. E., Davisson, M. T., Nusinowitz, S., Rengarajan, K., Boyd, A. P., Sidney, S. S., Phillips, M. J., Stewart, R. E., Chaudhury, R., Nickerson, J. M., Heckenlively, J. R., and Boatright, J. H. (2007) Two mouse retinal degenerations caused by missense mutations in the β-subunit of rod cGMP phosphodiesterase gene. *Vision Res.* **47,** 624–633 CrossRef Medline
28. Anant, J. S., Ong, O. C., Xie, H. Y., Clarke, S., O'Brien, P. J., and Fung, B. K. (1992) *In vivo* differential prenylation of retinal cyclic GMP phosphodiesterase catalytic subunits. *J. Biol. Chem.* **267,** 687–690 Medline
29. Goc, A., Chami, M., Lodowski, D. T., Bosshart, P., Moiseenkova-Bell, V., Baehr, W., Engel, A., and Palczewski, K. (2010) Structural characterization of the rod cGMP phosphodiesterase 6. *J. Mol. Biol.* **401,** 363–373 CrossRef Medline
30. Baehr, W., Devlin, M. J., and Applebury, M. L. (1979) Isolation and characterization of cGMP phosphodiesterase from bovine rod outer segments. *J. Biol. Chem.* **254,** 11669–11677 Medline
31. Hurley, J. B., Barry, B., and Ebrey, T. G. (1981) Isolation of an inhibitory protein for the cyclic guanosine 3′,5′-monophosphate phosphodiesterase of bovine rod outer segments. *Biochim. Biophys. Acta* **675,** 359–365 CrossRef Medline
32. Arshavsky, V. Y., Dumke, C. L., and Bownds, M. D. (1992) Noncatalytic cGMP-binding sites of amphibian rod cGMP phosphodiesterase control interaction with its inhibitory γ-subunits. A putative regulatory mechanism of the rod photoresponse. *J. Biol. Chem.* **267,** 24501–24507 Medline
33. Cote, R. H., and Brunnock, M. A. (1993) Intracellular cGMP concentration in rod photoreceptors is regulated by binding to high and moderate affinity cGMP binding sites. *J. Biol. Chem.* **268,** 17190–17198 Medline
34. Schnetkamp, P. P., Jalloul, A. H., Liu, G., and Szerencsei, R. T. (2014) The SLC24 family of K^+-dependent Na^+-$Ca2^+$ exchangers: structure-function relationships. *Curr. Top. Membr.* **73,** 263–287 CrossRef Medline
35. Vinberg, F., Wang, T., De Maria, A., Zhao, H., Bassnett, S., Chen, J., and Kefalov, V. J. (2017) The Na^+/Ca^{2+}, K^+ exchanger NCKX4 is required for efficient cone-mediated vision. *Elife* **6,** e24550 CrossRef Medline
36. Boye, S. L., Peterson, J. J., Choudhury, S., Min, S. H., Ruan, Q., McCullough, K. T., Zhang, Z., Olshevskaya, E. V., Peshenko, I. V., Hauswirth, W. W., Ding, X. Q., Dizhoor, A. M., and Boye, S. E. (2015) Gene therapy fully restores vision to the All-Cone Nrl(−/−) Gucy2e(−/−) mouse model of Leber congenital amaurosis-1. *Hum. Gene Ther.* **26,** 575–592 CrossRef Medline
37. Chen, C. K., Woodruff, M. L., Chen, F. S., Chen, Y., Cilluffo, M. C., Tranchina, D., and Fain, G. L. (2012) Modulation of mouse rod response decay by rhodopsin kinase and recoverin. *J. Neurosci.* **32,** 15998–16006 CrossRef Medline
38. Nikonov, S., Lamb, T. D., and Pugh, E. N., Jr. (2000) The role of steady phosphodiesterase activity in the kinetics and sensitivity of the light-adapted salamander rod photoresponse. *J. Gen. Physiol.* **116,** 795–824 CrossRef Medline
39. Krispel, C. M., Chen, D., Melling, N., Chen, Y. J., Martemyanov, K. A., Quillinan, N., Arshavsky, V. Y., Wensel, T. G., Chen, C. K., and Burns, M. E. (2006) RGS expression rate-limits recovery of rod photoresponses. *Neuron* **51,** 409–416 CrossRef Medline
40. Chen, C. K., Woodruff, M. L., Chen, F. S., Chen, D., and Fain, G. L. (2010) Background light produces a recoverin-dependent modulation of activated-rhodopsin lifetime in mouse rods. *J. Neurosci.* **30,** 1213–1220 CrossRef Medline
41. Pugh, E. N., Jr., and Lamb, T. D. (1993) Amplification and kinetics of the activation steps in phototransduction. *Biochim. Biophys. Acta* **1141,** 111–149 CrossRef Medline

42. Field, G. D., and Rieke, F. (2002) Mechanisms regulating variability of the single photon responses of mammalian rod photoreceptors. *Neuron* **35,** 733–747 CrossRef Medline
43. Nikonov, S. S., Kholodenko, R., Lem, J., and Pugh, E. N., Jr. (2006) Physiological features of the S- and M-cone photoreceptors of wild-type mice from single-cell recordings. *J. Gen. Physiol.* **127,** 359–374 CrossRef Medline
44. Reingruber, J., Pahlberg, J., Woodruff, M. L., Sampath, A. P., Fain, G. L., and Holcman, D. (2013) Detection of single photons by toad and mouse rods. *Proc. Natl. Acad. Sci. U.S.A.* **110,** 19378–19383 CrossRef Medline
45. Hamer, R. D., Nicholas, S. C., Tranchina, D., Lamb, T. D., and Jarvinen, J. L. (2005) Toward a unified model of vertebrate rod phototransduction. *Vis. Neurosci.* **22,** 417–436 CrossRef Medline
46. Chen, J., Woodruff, M. L., Wang, T., Concepcion, F. A., Tranchina, D., and Fain, G. L. (2010) Channel modulation and the mechanism of light adaptation in mouse rods. *J. Neurosci.* **30,** 16232–16240 CrossRef Medline
47. Hüttl, S., Michalakis, S., Seeliger, M., Luo, D. G., Acar, N., Geiger, H., Hudl, K., Mader, R., Haverkamp, S., Moser, M., Pfeifer, A., Gerstner, A., Yau, K. W., and Biel, M. (2005) Impaired channel targeting and retinal degeneration in mice lacking the cyclic nucleotide-gated channel subunit CNGB1. *J. Neurosci.* **25,** 130–138 CrossRef Medline
48. Zhang, Y., Molday, L. L., Molday, R. S., Sarfare, S. S., Woodruff, M. L., Fain, G. L., Kraft, T. W., and Pittler, S. J. (2009) Knockout of GARPs and the β-subunit of the rod cGMP-gated channel disrupts disk morphogenesis and rod outer segment structural integrity. *J. Cell Sci.* **122,** 1192–1200 CrossRef Medline
49. Baylor, D. A., and Nunn, B. J. (1986) Electrical properties of the light-sensitive conductance of rods of the salamander *Ambystoma tigrinum*. *J. Physiol.* **371,** 115–145 CrossRef Medline
50. Cheguru, P., Zhang, Z., and Artemyev, N. O. (2014) The GAFa domain of phosphodiesterase-6 contains a rod outer segment localization signal. *J. Neurochem.* **129,** 256–263 CrossRef Medline
51. Koch, S., Sothilingam, V., Garcia Garrido, M., Tanimoto, N., Becirovic, E., Koch, F., Seide, C., Beck, S. C., Seeliger, M. W., Biel, M., Mühlfriedel, R., and Michalakis, S. (2012) Gene therapy restores vision and delays degeneration in the CNGB1(−/−) mouse model of retinitis pigmentosa. *Hum. Mol. Genet.* **21,** 4486–4496 CrossRef Medline
52. Liu, X., Bulgakov, O. V., Wen, X. H., Woodruff, M. L., Pawlyk, B., Yang, J., Fain, G. L., Sandberg, M. A., Makino, C. L., and Li, T. (2004) AIPL1, the protein that is defective in Leber congenital amaurosis, is essential for the biosynthesis of retinal rod cGMP phosphodiesterase. *Proc. Natl. Acad. Sci. U.S.A.* **101,** 13903–13908 CrossRef Medline
53. Makino, C. L., Wen, X. H., Michaud, N., Peshenko, I. V., Pawlyk, B., Brush, R. S., Soloviev, M., Liu, X., Woodruff, M. L., Calvert, P. D., Savchenko, A. B., Anderson, R. E., Fain, G. L., Li, T., Sandberg, M. A., and Dizhoor, A. M. (2006) Effects of low AIPL1 expression on phototransduction in rods. *Invest. Ophthalmol. Vis. Sci.* **47,** 2185–2194 CrossRef Medline
54. Faktorovich, E. G., Steinberg, R. H., Yasumura, D., Matthes, M. T., and LaVail, M. M. (1990) Photoreceptor degeneration in inherited retinal dystrophy delayed by basic fibroblast growth factor. *Nature* **347,** 83–86 CrossRef Medline
55. Léveillard, T., Mohand-Saïd, S., Lorentz, O., Hicks, D., Fintz, A. C., Clérin, E., Simonutti, M., Forster, V., Cavusoglu, N., Chalmel, F., Dollé, P., Poch, O., Lambrou, G., and Sahel, J. A. (2004) Identification and characterization of rod-derived cone viability factor. *Nat. Genet.* **36,** 755–759 CrossRef Medline
56. Farber, D. B., and Lolley, R. N. (1974) Cyclic guanosine monophosphate: elevation in degenerating photoreceptor cells of the C3H mouse retina. *Science* **186,** 449–451 CrossRef Medline
57. Cronin, T., Lyubarsky, A., and Bennett, J. (2012) Dark-rearing the rd10 mouse: implications for therapy. *Adv. Exp. Med. Biol.* **723,** 129–136 CrossRef Medline
58. Dong, E., Bachleda, A., Xiong, Y., Osawa, S., and Weiss, E. R. (2017) Reduced phosphoCREB in Muller glia during retinal degeneration in rd10 mice. *Mol. Vis.* **23,** 90–102 CrossRef Medline
59. Wang, T., and Chen, J. (2014) Induction of the unfolded protein response by constitutive G-protein signaling in rod photoreceptor cells. *J. Biol. Chem.* **289,** 29310–29321 CrossRef Medline
60. Baylor, D. A., Lamb, T. D., and Yau, K. W. (1979) The membrane current of single rod outer segments. *J. Physiol.* **288,** 589–611 Medline
61. Nymark, S., Frederiksen, R., Woodruff, M. L., Cornwall, M. C., and Fain, G. L. (2012) Bleaching of mouse rods: microspectrophotometry and suction-electrode recording. *J. Physiol.* **590,** 2353–2364 CrossRef Medline
62. Chen, C. K., Woodruff, M. L., and Fain, G. L. (2015) Rhodopsin kinase and recoverin modulate phosphodiesterase during mouse photoreceptor light adaptation. *J. Gen. Physiol.* **145,** 213–224 CrossRef Medline